LAWRENCE
LIVERMORE
NATIONAL
LABORATORY

UCRL-PROC-206102

EFFECT OF NITRATE ON THE REPASSIVATION POTENTIAL OF ALLOY 22 IN CHLORIDE CONTAINING ENVIRONMENTS.

G.O.Ilevbare, K.J. King, S.R. Gordon, H.A. Elayat, G.E. Gdowski, T.S.E. Summers

August 17, 2004

206th Meeting Of the Electrochemical Society
Honolulu, HI, United States
October 3, 2004 through October 8, 2004

EFFECT OF NITRATE ON THE REPASSIVATION POTENTIAL OF ALLOY 22 IN CHLORIDE CONTAINING ENVIRONMENTS.

G. O. Ilevbare, K.J. King, S.R. Gordon, H.A. Elayat, G.E. Gdowski, and T.S.E. Summers
Lawrence Livermore National Laboratory, 7000 East Avenue, Livermore, California 94550, USA

ABSTRACT

The study of Alloy 22 was undertaken in several selected nitrate/chloride (NO_3^-/Cl^-) electrolytes with chloride concentrations [Cl^-] of 1.0, 3.5 and 6.0 molal with [NO_3^-]/[Cl^-] ratios of 0.05, 0.15 and 0.5 at temperatures up to 100°C. Results showed that the repassivation potentials increased with increase in [NO_3^-]/[Cl^-] ratio and decreased with increase in temperature. The absolute [Cl^-] was found to have less of an effect on the repassivation potential compared with temperature and the NO_3^-/Cl^-. Regression analyses were carried out and expressions were derived to describe the relationship between the repassivation potential, temperature, [Cl^-] and [NO_3^-] for the conditions tested.

INTRODUCTION

Alloy 22 (N06022) is a nickel (Ni)- alloy that contains 22% chromium (Cr), 13% molybdenum (Mo), 3% tungsten (W) and about 3% iron (Fe) (Table 1). Alloy 22 possesses outstanding corrosion resistance characteristics and maintains its passivity in most industrial environments. Alloy 22 exhibits remarkably low general corrosion rates, as well as exceptional resistance to localized corrosion, including environmentally assisted cracking [1-7]. As a result, it has become an alloy of choice for numerous industrial applications including underground waste disposal systems.

Nitrate is a known inhibitor of pitting and crevice corrosion as well as stress corrosion cracking in stainless steels and Ni-alloys [8-29]. On occasion NO_3^- has been found to be better than SO_4^{2-} and CrO_4^{2-} in inhibiting localized corrosion in stainless steels [16-19]. NO_3^- has also been found to be more effective in the more highly alloyed steels suggesting synergy between NO_3^- and elements like Mo in inhibition [20]. It would be expect that such synergistic effect might also occur with highly alloyed Ni-alloys too.

An interesting observation made by numerous authors about NO_3^- inhibition is the existence of a high passivation potential [8, 26-28]. It has also been suggested that there is a system dependent critical passivation potential below which inhibition of localized corrosion by NO_3^- will not take place [26]. Others have defined this critical potential as the potential above which the sample remains steadily passive or transpassive [8, 24, 26, 27]. This threshold passivating potential decreases as the amount of NO_3^- in solution increases [24, 26].

While there is general agreement about the efficacy of NO_3^- in inhibiting localized corrosion in SS and Ni-alloys, there is no such consensus with regard to the mechanism of action of NO_3^-. A good number of the early and a few more recent mechanisms were

based on the theory of competitive adsorption [9, 10, 16, 18, 20]. In these mechanisms, NO_3^- simply adsorbed to weak sites on the oxide film to prevent the incorporation of aggressive ions like Cl^- at these sites, thus averting or delaying dissolution and promoting oxide film growth. However, the small amounts of NO_3^- required to produce significant changes in pitting or crevice potentials, especially when compared with other oxyanions whose efficacy might be more favored by competitive adsorption (e.g. SO_4^{2-}), suggests that other chemical processes might be involved in the inhibition mechanism of NO_3^-.

The electro-reduction of NO_3^- to NH_4^+ (possibly through a NO_2^- intermediate) has also been suggested as a possible inhibition mechanism for NO_3^- [23, 26, 33-35]. Two of such reduction reactions are described in Equations 1 and 2 as follows:

$$NO_3^- + 10H^+ + 8e^- \rightarrow 3H_2O + NH_4^+ \qquad [1]$$

$$NO_3^- + Fe^{2+} + 2H^+ \rightarrow NO_2^- + Fe^{3+} + H_2O \qquad [2]$$

These mechanisms involve the consumption of H+ (and production of water) with resulting nucleation or formation of a stable passivity by a redox reaction (possibly in conjunction with Fe^{2+}) within the precipitated salt film at the bottom of a pit or crevice [23, 26, 33-36]. However, the reduction of NO_3^- takes place at potentials much lower than the passivation (threshold) potential where inhibition occurs in many cases. This suggests that the question as to why high critical passivation potentials are required in NO_3^- inhibition may still remain an open one.

Another suggested mechanism involves the reduction of NO_3^- to atomic nitrogen [23, 28, 34, 35]. The N that is formed may then proceeds to adsorb to a de-passivated metal surface (or to weak points on the oxide film) to promote oxide film formation [35]. Thus, N may act as an anodic site blocker in the very early stages of pit development [35]. It has also been suggested that the elemental N might be able to undergo reduction to ammonium (NH_4^+) ions in a reaction analogous to Equation 1 as follows:

$$N + 4H^+ + 3e^- \rightarrow NH_4^+ \qquad [3]$$

This reaction also involves the consumption of acid, which consequently increases local pH. Indeed, numerous workers have detected NH_4^+ in solution after growth of corrosion pits and cracks on SS alloyed with N [28, 37-39]. However, others have found no evidence of NH_4^+, NO_2^-, or any reduction product of NO_3^- in pits or crevices on stainless steels when NO_3^- was used as an inhibitor, nor on N-containing stainless steel [17, 40]).

One of the goals of this study was to determine the effect of NO_3^- on the crevice repasssivation potential of Alloy 22. To achieve this, carefully designed statistical test matrixes covering the selected range of Cl^- and NO_3^- compositions as well as temperatures were employed in carrying out the experiments. Specimens for these experiments were in the form of multiple crevice assemblies (MCA). Tests in this investigation included open circuit potential monitoring, polarization resistance and cyclic polarization experiments.

EXPERIMENTAL PROCEDURE

Multiple Crevice Assembly (MCA) specimens (Figure 1) were fabricated from welded 3.175 cm (1.25 inches) thick Alloy 22 (N06022) plates. The welds were made by means of Gas Tungsten Arc Welding (GTAW). The double-U shaped welds were completed in about 8-10 passes (Figure 2). The weld metal in the welded specimens was taken from the outermost portion (surface) of the welds. Since the welds had a double-U configuration, this meant that the volume of weld metal on the sample was not the same throughout the ~2 mm thickness of the samples. Nonetheless, the amount of weld metal on the samples covered an area on the working surface that was at least 1 cm wide and extended across the entire face (perpendicular to the stem of the specimen) of the specimen on which the crevice formers were assembled. The chemical composition of the 3.175 cm plate as documented by the supplier appears in Table 1. The composition is consistent with ASTM-B 575 (for plates/sheets) standard [41, 42]. The composition of the filler metal was taken before it was used in the welding process.

The MCA design was optimized for crevice corrosion studies so that most of the working surface was covered by the ceramic crevice former. The working surfaces of the MCA specimens were finish with 600-grit silicon carbide (SiC) paper. The edge of the specimens (surface 90 degrees in angle to the working surface) was also finished with 600-grit SiC paper after first grinding with 100 and then 240-grit SiC paper to remove all damaged portions of the sample caused by the electro discharge machine (EDM) during the fabrication process. All the grinding was carried out wet. After grinding, the specimens were degreased first with hexane, then with acetone and followed by methanol. The rest of the MCA consisted of titanium (Ti) grade 2 nuts, bolts and washers, as well as ceramic crevice formers with multiple ridges (also referred to as teeth). The bolts were polytetrafluoroethylene (PTFE) wrapped to prevent these hardware components from coming into electrical contact with the specimen. Each crevice former had a total of 12 ridges (or teeth) on it, creating 12 different potential crevice sites on each face of the specimen, and a total of 24 potential sites in each assembly (Figure 1). The assembly was tightened to a torque of 70 in-lb. PTFE tape inserts were placed between the ceramic crevice former and the MCA specimen prior to tightening. This was done to fill in the micro voids created by the micro-rough surfaces of the specimen and the ceramic crevice former, and to increase the reproducibly of the tight crevices in all specimens. The total surface area of the MCA specimen immersed in the electrolyte was 7.43 cm^2. This surface area included the area under the 24 ridges of the crevice formers, which had a combined surface area of 1.6 cm^2. In current density estimations, the surface area of 7.43 cm^2 was used for calculations.

A three-electrode cell with a capacity of 1000 cm^3 was used for experimentation. The volume of electrolyte in the cell was ~900 cm^3. A saturated silver/silver chloride (SSC) (Ag/AgCl) electrode was the reference electrode (RE). The RE was maintained near room temperature by mounting it onto the end of a water-cooled Luggin probe. The temperature of the water pumped through the cooling jacket of the Luggin probe was between 5 and 12 ^oC. Thermal liquid junction calculations showed that potential variation caused by this phenomenon was in the order of a few mV (~10 mV maximum). Also, according to Macdonald et al., a high KCl concentration in the reference electrode tends to suppress thermal liquid junction potentials across the boundary between the high and low temperature solutions [43]. Liquid junction potential variations were therefore

ignored in further analyses. The counter electrode was made of a 40 cm^2 platinum (Pt) foil. The temperature of the electrolyte was maintained with an oil-filled heating bath. The specimen was immersed into the cell immediately after the grinding process with the electrolyte at the desired test temperature. Electrolyte temperature readings were taken before and after the experiment with a thermocouple. Electrochemical measurements were carried with a potentiostat. The corrosion (open circuit) potential (E_{corr}) was monitored for 24 hours, which allowed E_{corr} to settle considerably. This was followed by polarization resistance measurements, and then by cyclic potentiodynamic polarization measurements immediately afterwards. Scans at 0.1667mVs^{-1} (600 mVh^{-1}) between -20 and +20 mV relative to the E_{corr} were carried out for polarization resistance measurements. Corrosion rates were calculated from the values derived from these polarization resistance measurements. Cyclic polarization was started approximately 100 mV below E_{corr}, and continued until the current density from the specimen reached a maximum of up to 5 $mAcm^{-2}$, or up to 0.6 V (SSC) before reversal of the scan unless otherwise stated. The sweep rate in the forward and reverse directions was 0.1667 mVs^{-1}.

A carefully designed statistical test matrix was employed in carrying out these investigations. The electrolytes used in these experiments included 1.0, 3.5 and 6.0 molal (m), with KNO_3 addition to give $[NO_3^-]/[Cl^-]$ ratios of 0.05, 0.15 and 0.5. These gave a combination of 9 different electrolytes as shown in Table 2. All the electrolytes had a pH of between 5 and 5.50 at room temperature. The experiments were carried out at 60, 80 and 100 ^oC. Two repeat experiments were performed at each experimental condition, resulting in a total compliment of 54 tests which were carried out in a predetermined random order to eliminate any extraneous errors that might be introduced by the experimental set up or other external factors. All electrolytes were deaerated with nitrogen gas (N_2). N_2 was bubbled through the electrolytes for at least one hour before and throughout the experiments at a rate of ~100 cc per minute. All electrolytes were prepared using certified American Chemical Society (ACS) reagent grade chemicals.

EXPERIMENTAL RESULTS

The Corrosion Potential (E_{corr})

The corrosion potential (E_{corr}) of Alloy 22 decreased with time at all temperatures in all the nine (9) electrolytes tested over the 24-hour monitoring period. Figure 3 shows representative curves of Alloy 22 with 1, 3.5 and 6.0 m with NO_3^- additions equivalent to a 0.05 $[NO_3^-]/[Cl^-]$ ratio. Figure 4 shows the corrosion potential of Alloy 22 in the 27 environments (9 electrolyte at 3 temperatures) tested. The data points in Figure 4 represent individual values, and the curve fits are interpolations (averages) between the two data points presented for each condition. Figure 4 suggests that neither $[Cl^-]$, $[NO_3^-]/[Cl^-]$ ratio nor temperature affected E_{corr} of Alloy 22 in the range investigated.

The Passive Corrosion Rate (CR)

Corrosion rates were calculated from polarization resistance values obtained from short scans (-20 to +20 mV) relative to E_{corr} according to the ASTM G 59 method [44]. Upon completion of the scans, liner fits were carried out between the potentials of -10 and +10 mV relative to E_{corr}. A value of ±0.12 V/decade was assumed for the Tafel constants β_a nd β_c for the anodic and cathodic curves respectively. Thus, the values obtained from the calculations (Equation 4) are approximations of the corrosion rates.

$$CR = k\frac{i_{corr}}{\rho}EW \qquad [4]$$

Where ***CR*** is the corrosion rate in microns per year, ***k*** is a unit conversion factor to microns per year (3.27×10^6 $\mu m.g.A^{-1}.cm^{-1}.yr^{-1}$), i_{corr} is the measured corrosion current density; ***EW*** is the equivalent weight of Alloy 22 (23.38) assuming an equivalent dissolution of major alloying elements as Ni^{2+}, Cr^{3+}, Mo^{6+}, Fe^{2+} and W^{6+}; and $\boldsymbol{\rho}$ is the density of Alloy 22 (8.69 $g.cm^{-3}$) [45]. These corrosion rates represent metal dissolution under passive conditions at potentials close to open circuit conditions.

In Figure 5, each data point represents values from 3 repeat experiments carried out in succession after a 24-hour exposure without renewing or resurfacing the specimen after each measurement. There are 2 data points for every condition, and the curve fits are interpolations between the two points. Figures 5a-5c show that neither $[Cl^-]$ nor $[NO_3^-]/[Cl^-]$ ratio affects the corrosion rate of Alloy 22. This is consistent with the observation that these factors also had no effect on E_{corr}. However, Figure 5 shows that the passive corrosion rate of Alloy 22 increases with temperature. The highest corrosion rate values observed were at 100°C in electrolytes 1 and 9 (0.96 and 0.85$\mu m.yr^{-1}$ respectively). These electrolytes have compositions of 1.0 m Cl^- + 0.05 m NO_3^-, and 6.0 m Cl^- + 3.0 m NO_3^- respectively, and support the observation that temperature rather than electrolyte composition was the dominant factor that determined the corrosion rate in the conditions tested.

Crevice Repassivation Potential (E_{r1})

E_{r1} was the potential that coincided with a current density of 1×10^{-6} Acm^{-2} on the reverse scan of the polarization curve. In addition, for an E_{r1} value to be included in the analyses, there must be an observable hysteresis loop in the polarization curve. Figures 6a, 6b and 6c show representative polarization curves for Alloy 22 in 1 m NaCl with KNO_3 additions 0.05, 0.15 and 0.5 m respectively, representing NO_3^- to Cl^- ratio of 0.05, 0.15 and 0.5 respectively. Under the analyses criteria, Figure 6c (E_{r1} = 0.504 V_{SSC}) was not included in any of the analyses for the repassivation potential because of the absence of a hysteresis loop. None of such curves (as in Figure 6c) showed any signs of crevice current under an optical microscope examination.

The shapes of the polarization curves of Alloy 22 were similar when the $[NO_3^-]/[Cl^-]$ ratio of solute in the electrolyte was the same. Consequently, Figures 6a, 6b and 6c are representative of the polarization curves of Alloy 22 taken in the solutions containing 3.5 and 6.0 m Cl^- at the same $[NO_3^-]/[Cl^-]$ ratio. Thus, the $[NO_3^-]/[Cl^-]$ ratio rather than $[Cl^-]$ was a more dominant effect on the behavior of Alloy 22. It can be seen from Figure 6 that the size of the hysterisis loop decreased as the $[NO_3^-]/[Cl^-]$ ratio, and hence as the amount of NO_3^- increased. Generally, it was observed that the degree of damage on a specimen decreased as the size of the hysterisis loop decreased. This is reasonable since the size of the hysterisis loop tends to be proportional to the amount of charge passed, and hence to the amount of metal dissolution which occurred.

Figure 6d shows a photo of the creviced area on Alloy 22 in 1 m NaCl + 0.05 m KNO_3 at 60°C (Figure 6a). It shows that crevice corrosion initiated and propagated underneath the crevice former, suggesting that the crevice former was still required as a barrier to diffusion throughout the propagation this crevice. This behavior of crevice propagation was representative of all the condition tested in this study, that is, all the crevice

propagation started as individual pits, and propagation was limited to underneath the crevice former. This is quite different from observations made in 5 M $CaCl_2$ where propagation proceeds outside the crevice former once the initiation and early propagation stage were over [46].

Figure 7 shows the repassivation potential as a function of $[NO_3^-]/[Cl^-]$ ratio at all $[Cl^-]$ and temperatures tested. Figure 7 shows that the repasivation potential increased with $[NO_3^-]/[Cl^-]$ ratio (and hence with $[NO_3^-]$) and as temperature decreased. Figure 8 shows the repassivation potential as a function of $[Cl^-]$ at all three $[NO_3^-]/[Cl^-]$ ratios and temperatures tested. Figure 8 shows that the repassivation potential shows a weak dependence (if any) on $[Cl^-]$ and a strong dependence on the $[NO_3^-]/[Cl^-]$ ratio.

A regression analysis of the repassivation potential data was carried out in order to derive a model for the observed behavior of Alloy 22 in these environments. From three levels of temperature, $[Cl^-]$ and $[NO_3^-]/[Cl^-]$ ratios the following model was derived:

$$E_{r1} = 1.0843 - 0.0635\log[Cl^-] - 0.0071T + 0.361\log\frac{[NO_3^-]}{[Cl^-]} \qquad [5]$$

The regression coefficient, R^2, was 0.745. Analyses showed that there was no multi co-linearity between the independent variables (temperature, $[Cl^-]$ and $[NO_3^-]/[Cl^-]$ ratios) in this equation, implying there was no co-dependence of these variables. The distribution of the standardized residuals was close to normal. The model fitted the dated reasonably well. This is illustrated in Figures 9 and 10. Figure 9 shows the lines of fit from the model in relation to actual data points in a graph of the repassivation potential as a function of $[NO_3^-]/[Cl^-]$ ratio at 1.0, 3.5 and 6.0 m Cl^- at 100°C. Figure 10 is a 3-D representation of the repassivation potential as a function of $[Cl^-]$ and $[NO_3^-]$ at 100 °C. The surface is derived from the regression analyses. Included in Figure 10 are experimental data points from the environments tested at 100 °C (with $[Cl^-]$ of 1.0, 3.5 and 6.0 molal and $[NO_3^-]/[Cl^-]$ ratio of 0.05, 0.15 and 0.5). As seen from Figures 9and 10, the repassivation potential is predicted to rise with increase in $[NO_3^-]$ and with decrease $[Cl^-]$, although the effect of $[Cl^-]$ tends to be less significant.

DISCUSSION

The $[NO_3^-]$ employed in this work spans a range that represents relatively low to high concentrations. The ten-fold difference in upper and lower bounds of NO_3^- affords the opportunity of observing the effect of NO_3^- at vastly different levels. Cl^- still remained the predominant anion in the electrolytes. For this reason, it is expected that the mechanisms of crevice initiation and indeed repassivation will not be significantly altered by the presence of NO_3^- at least at the lower concentrations.

The amount of NO_3^- used in the systems employed did not significantly affect the corrosion potential or passive corrosion rate of Alloy 22 (Figures 4 and 5). Similar corrosion potentials correlated to similar values for the passive corrosion rate, although the latter exhibited a slight temperature dependence. This is reasonable since the average kinetic energy of ions increases with increase in temperature and would translate to higher dissolution rates. The fact that NO_3^- had no significant effect on the passive

corrosion rate suggests that the mechanisms of inhibition of NO_3^- on Alloy 22 might not be primarily associated with the improvement of the passive oxide film in the systems studies. A significant reduction in the passive corrosion rate of Alloy 22, probably accompanied by an increase in the corrosion potential would have signified otherwise. This might suggest that mechanism solely based on the adsorption NO_3^- or atomic N (from reduction of NO_3^-) to weak sites on the oxide film to promote more robust oxide film growth at these points could be ruled out in this study. This observation is consistent with finding which showed that NO_3^- did not effect the rate of nucleation on SS 304 and 316 in solutions containing 0.1 M HCl + 0.01 M $NaNO_3$ [47]. Generally, a reduction in the number and rate of nucleation usually accompanies improvements in the integrity of the oxide film, or occur when an inhibitor strongly affects the ability of aggressive ions to penetrate the oxide film.

Earlier work [1, 48] showed that the repassivation potential is a more reproducible parameter compared with the crevice breakdown potential (E_{crit}). Some of the reasons for this include the fact that compared with the crevice breakdown potential, the repassivation potential is less affected by sweep rate, and is not dependent on the amount of charge passed, and hence on the amount of dissolution associated with crevice corrosion that has occurred. Consequently, the repassivation potential is a reliable parameter for the study of the effect of NO_3^- on the localized corrosion in Alloy 22.

Figure 6d (SEM photo) suggests that the mechanism of crevice initiation involves the formation of pits, which then coalesce into trenches under the creviced area. The reduction in the size of the hysteresis loop and the accompanying reduction of the amount of dissolution between crevice initiation and crevice repassivation as $[NO_3^-]$ increases shows that NO_3^- inhibited crevice corrosion in Alloy 22. This is consistent with the increase in the repassivation potential as the $[NO_3^-]/[Cl^-]$ ratio increases, and hence as $[NO_3^-]$ increases. Given that the amount of charge passed (i.e., the amount of dissolution that occurs) tends not to affect the repassivaiton potential of Alloy 22 significantly [1], the increases observed in the repassivation potential of Alloy 22 are undoubtedly associated with the ability of NO_3^- to more quickly bring about the cessation of dissolution with the crevice upon the reversal of potential.

The absence of a significant effect of Cl^- on the repassivation potential (Figure 8) is likely due to the fact that it is the $[Cl^-]$ in the crevice, and the accompanying reaction within the crevice that dominate and control the repassivation process, rather than the $[Cl^-]$ in the bulk solution. Therefore, once a crevice is self-sustaining, it is not expected that the concentration of the bulk electrolyte will play a significant role in the repassivation process.

CONCLUSIONS

1. The repassivation potential (E_{r1}) increased with $[NO3^-]/[Cl^-]$ ratio between 60 and 100°C in the electrolytes tested.
2. The $[NO3^-]/[Cl^-]$ ratio and temperature had a more dominant effect on E_{r1} compared $[Cl^-]$ with had little or no effect on E_{r1}.

3. The $[NO_3^-]/[Cl^-]$ ratio had no significant effect on E_{corr} as CR between 60 and 100°C. However, CR showed a temperature dependence between 60 and 100°C in the electrolytes tested.

ACKNOWLEDGEMENTS

The Department of Energy Office of Civilian Radioactive Waste Management (OCRWM) sponsored this work. This work was done under the auspices of the U.S. Department of Energy (DOE) by the University of California, Lawrence Livermore National Laboratory (LLNL) under contract No. W-7405-Eng-48. This work is supported by the Yucca Mountain Project, LLNL.

REFERENCES

1. B. A. Kehler, G.O. Ilevbare and J.R. Scully Corrosion, **57**, 1042, (2001).
2. B. A. Kehler, G. O. Ilevbare and J. R. Scully in Corrosion 2001, Crevice Corrosion Behavior, of Ni-Cr-Mo Alloys: Comparison of Alloys 625 and 22, the proceedings of NACE Topical Research Symposium, p.30, March 2001.
3. Haynes International, Inc., Product Brochure H-200B, Haynes International Inc. Kokomo, IN, p.15, 1987.
4. Haynes International, Inc., Product Brochure H-2019C, Haynes International Inc. Kokomo, IN, p.22, 1988.
5. G.O. Ilevbare T. Lian and J.C. Farmer, Paper No. 02539, Corrosion 2002.
6. K.A. Gruss, G.A. Cragnolio, D.S. Dunn and N.Sridhar, Corrosion '98, Paper No. 149, 1998.
7. S.J. Lukezich, The Corrosion Behavior of Ni-Base High Performance Alloys in Simulated Repository Environments, MS Thesis, The Ohio State University 1989.
8. W. Schwenk, Corrosion, **20**, 129t (1964).
9. H.H. Uhlig and J.R. Gilman, Corrosion, **20**, 289t (1964).
10. H.P. Leckie and H.H. Uhlig, J. Electrochem. Soc., **113**, 1262, (1966).
11. R.M. Saleh, M.M. Badran, A.A. El Hosary and H.A. El Dahan, British Corrosion Journal, **23,** 105 (1988).
12. H.S. Tong and D.J. Swartz, Corrosion, **36**, 699 (1980).
13. H.C. Man and D.R.Gabe, Corrosion Science, **21**, 713 (1981).
14. A. Hirano, N. Aoki and T. Kurosawa, Corrosion, **39**, 313 (1983).
15. G.A. Cragnolino and N Shridhar, Corrosion, **47**, 464, (1991).
16. I.L Rozenfeld and I.S. Danilov, Corrosion Science, **7**, 129 (1967).
17. C.S Brossia and R. G Kelly, Corrosion, **54**, 145 (1998).
18. H.A. El Dahan, Journal of Materials Science, **34**, 851(1999).
19. H.A. El Dahan, Journal of Materials Science, **34**, 859(1999).
20. M.A. Streicher, J. Electrochemical Soc., **103**, 375 (1956).
21. V.I. Lomovstev, A.P. Gorodnichii and A.B. Bykov, Protection of metals, **29**, 28 (1993). Translated from Zashchita Metallov, **29**, 36 (1993).
22. S.S. Chatterjee and H.S. Mahanti in Corrosion and Maintenance, Oct-Dec, p.231, (1985).
23. R. Bandy and D. Van Rooyen, Corrosion, **39**, 227 (1983).
24. H.-H. Strehblow and B. Titze in Corrosion Science, **17**, 461 (1977).
25. D Herbert, G.O.H Whillock and S.E. Worthtington in Materials Science Forum, Electrochemical Methods in Corrosion Research V; Proceedings of the 5th International Symposium held in Sesimbra, Portugal, September 5-8 1994, Eds M.G.S. Ferreira and A.M.P. Simoes Vol. 192-194, p.469 (1995).
26. R.C. Newman, and M.A.A. Ajjawi, Corrosion Science, **26**, 1057 (1986).
27. J. Tousek, Collection of Czechoslovak Chemical Communications, **46**, 2834 (1981).
28. H. Yashiro, D. Hirayasu and N. Kumagai in ISIJ International, **42**, 1477 (2002).
29. R.M. Tennent in Science Data book Published by Oliver Boyd, Edinburgh (1987).
30. J.E. Huheey, in Inorganic Chemisty: Principles Structure and Reactivity, 2nd Edition, p.3:78, Haper and Row, New York. (1978).
31. J.E. Huheey, E.A Keither and R.L. Keither in Inorganic Chemisty: Principles Structure and Reactivity, 4th Edition, p4: 118, Haper Collins, New York (1993).

32. CRC Handbook of Chemistry and Physics Editor in Chief, D.R. Lide, 82nd edition, p. 5-96, CRC Press, Boca Raton Florida (2001).
33. L.I. Freiman, V.S. Novitskii, V.S. Kuzub and V.A. Makarov, Protection of Metals, **18**, 272 (1982). Translated from Zashchita Metallov, **18**, 359 (1982).
34. R.C. Newman and A.J. Betts in Advances in Localized Corrosion, Proceedings of the Second International. Conference on Localized Corrosion Eds: H.S. Isaacs, U. Bertocci, J. Kruger and S. Smialowska, June 1-5 1987 Orlando Florida. p. 271, NACE (1987),
35. R.C. Newman and T. Shahrabi, Corrosion Science, **27**, 827 (1987).
36. T.R. Beck J. Electrochem Soc., **129**, 2412 (1982).
37. R.F.A. Jagelius-Patterson, Corrosion Science, **41**, 1639 (1999).
38. H, Yashiro, A. Oyama and K. Tanno, Corrosion, **53**, 290, (1997).
39. W-T. Tsai, B. Reynders, M. Stratmann and H. J. Grabke, Corrosion Science, **34**, 1647 (1993).
40. K. Zagorski and A. Doraczynska, Corrosion Science, **16**, 405 (1976).
41. ASTM B574, Annual Book of ASTM Standards, Nonferrous Metal Products, Volume 02.04, p.531, American Society of Testing and Materials, West Conshohocken, PA (2000).
42. ASTM B575, Annual Book of ASTM Standards, Nonferrous Metal Products, Volume 02.04, p.535, American Society of Testing and Materials, West Conshohocken, PA (2000).
43. D.D. Macdonald, A.C. Scott, and P. Wentrcek, J. Electrochem. Soc., **126**, 908 (1978).
44. ASTM G59, ASTM Standards, Wear and Erosion; Metal Corrosion, Volume 03.02, American Society of Testing and Materials, West Conshohocken, PA (2001).
45. ASTM G 102, ASTM Standards, Wear and Erosion; Metal Corrosion, Volume 03.02, American Society of Testing and Materials, West Conshohocken, PA (2001).
46. G.O.Ilevbare, The Effect of Welding on the Breakdown and Repassivation Potentials of Alloy 22 in 5 M $CaCl_2$, UCRL-JC-155209, University of California Records Library, Lawrence Livermore National Laboratory.
47. G.O.Ilevbare, Inhibition of Pitting Corrosion in Stainless Steels, Thesis, The University of Cambridge, England, (1996).
48. G.O. Ilevbare, Unpublished work, LLNL

Table 1. Chemical composition of Alloy 22 (UNS No. N06022) given in weight percent.

Element	Actual Composition			ASTM Requirements ASTM B575-Sheets
	Wrought	Welded (Weld/Filler Metal)	Welded (Base Metal)	
Mo	14.10	14.00	13.82	12.5-14.5
Cr	22.00	20.54	20.38	20.0-22.5
Fe	4.50	2.08	2.85	2.0-6.0
W	2.70	3.10	2.64	2.5-3.5
Co	1.30	0.03	0.01	0.0-2.5
C	0.003	0.004	0.005	0.000-0.015
Si	0.03	0.06	0.05	0.00-0.08
Mn	0.31	0.20	0.16	0.00-0.50
V	0.16	0.03	0.171	0.00-0.35
P	0.01	0.004	0.008	0.00-0.02
S	<0.01	0.001	0.0002	0.00-0.02
Ni	Bal.	Bal.	Bal	Bal.

Wrought Specimens from Heat # 2277-5-3203. Welded Specimens: Base metal from Heat #059902LL1; Weld/filler metal from Heat # XX1753BG.

Table 2: Electrolyte compositions

Electrolyte	Concentration [Molal] Mol.kg^{-1}		Concentration [Molar] Mol.dm^{-3}		pH
	NaCl	KNO_3	NaCl	KNO_3	
1	1.0	0.050	0.96	0.05	5.38
2	1.0	0.150	0.95	0.15	5.13
3	1.0	0.500	0.94	0.47	5.32
4	3.5	0.175	3.08	0.15	5.53
5	3.5	0.525	3.04	0.46	5.49
6	3.5	1.750	2.91	1.45	5.49
7	6.0	0.300	4.95	0.25	5.40
8	6.0	0.900	4.86	0.73	5.37
9	6.0	3.000	4.59	2.29	5.36

Figure 1: Multiple Crevice Assembly (MCA), bottom. It shows the lollipop-like specimen (top), titanium grade two bolt (Teflon wrapped for electrical insulation), washers nut and ceramic washers

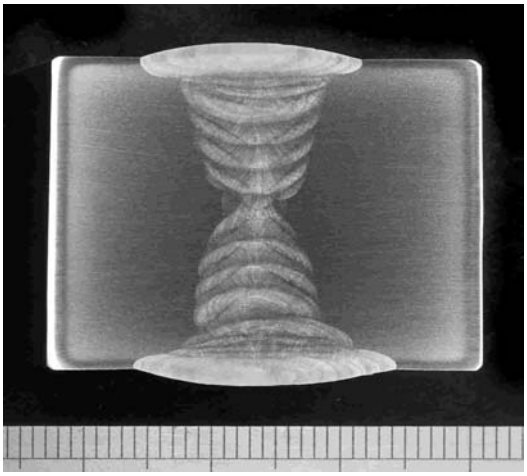

Figure 2. Cross-section of welded plate from which welded MCA samples were fabricated. Double-U weld was completed in 8-10 passes. The plate is 3.175 cm (1.25 inches) thick.

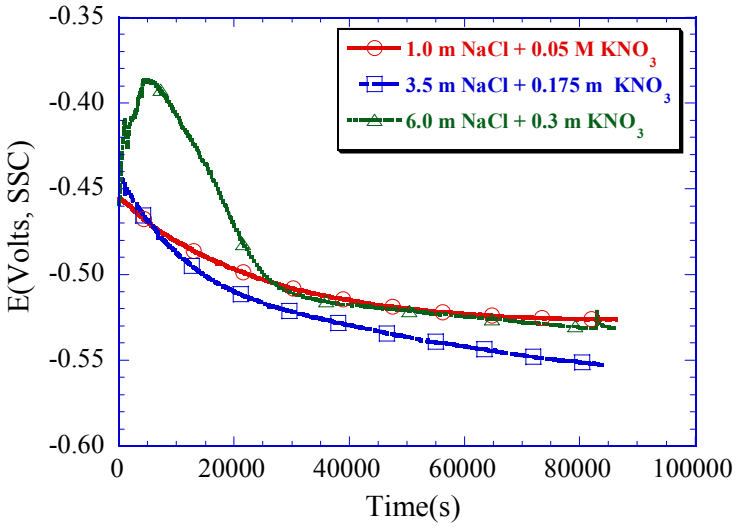

Figure 3. 24-hour corrosion potentials of Alloy 22 in 1 m NaCl + 0.05 m KNO_3, 3.5 m NaCl + 0.175 m KNO_3, and 6.0 m NaCl + 0.3 m KNO_3, at 100 ^{o}C.

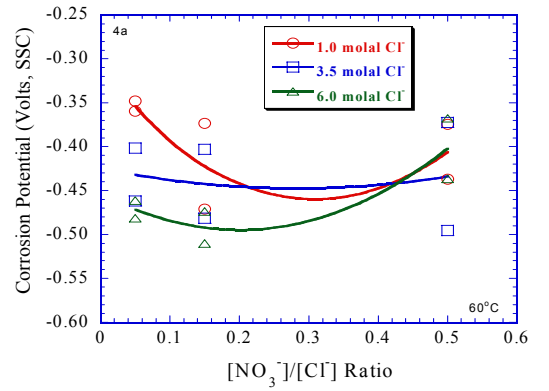

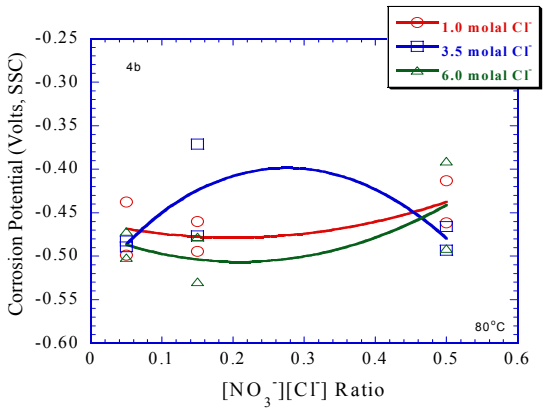

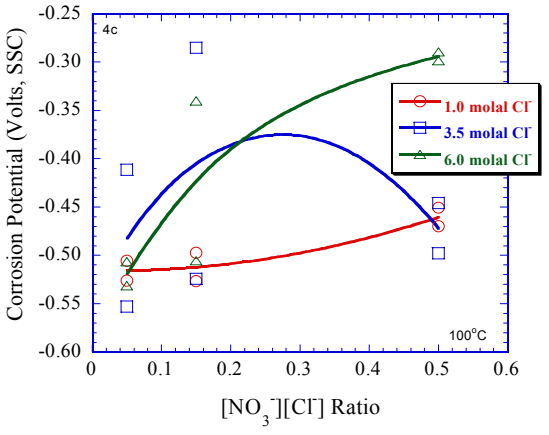

Figure 4. 24-hour Corrosion potentials as a function of $[NO_3^-]/[Cl^-]$ ratio for 1.0, 3.5, and 6.0 m Cl^- at 60(4a), 80(4b) and 100°C(4c)

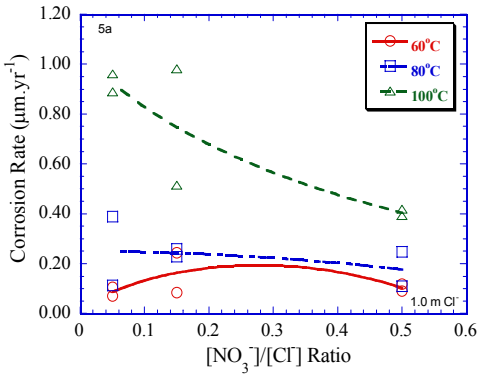

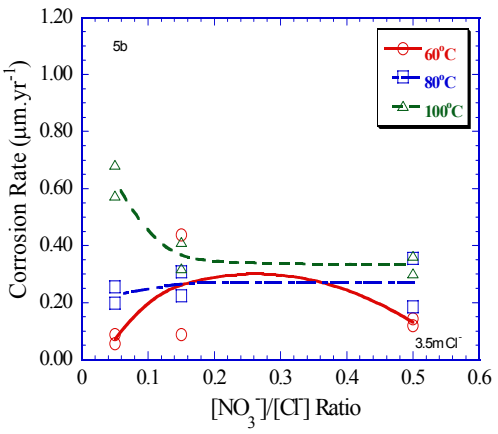

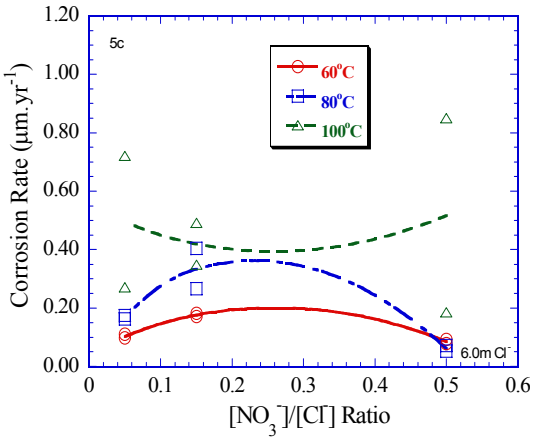

Figure 5. Passive corrosion rates of Alloy 22 after a 24-hour immersion in the electrolytes used (Table 2) as a function of $[NO_3^-]/[Cl^-]$ ratio for 1.0 (5a), 3.5 (5b), and 6.0 m Cl^- (5c) at 60, 80 and 100°C

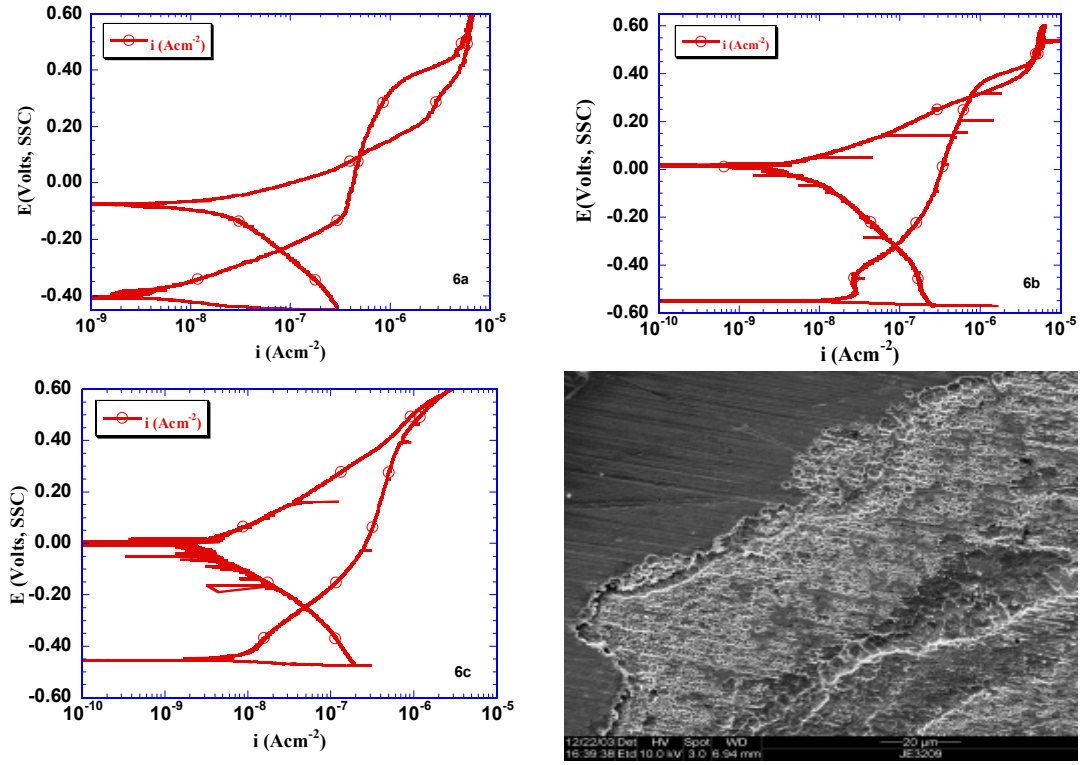

Figure 6. Polarization curves for Alloy 22 in 1 m NaCl with KNO_3 additions (6a) 0.05, (6b) 0.15 and (6c) 0.5 m respectively, representing NO_3^- to Cl^- ratio of 0.05, 0.15 and 0.5 respectively; and (6d) a photo (SEM) of the creviced area on Alloy 22 in 1 m NaCl + 0.05 M KNO_3 at 60°C.

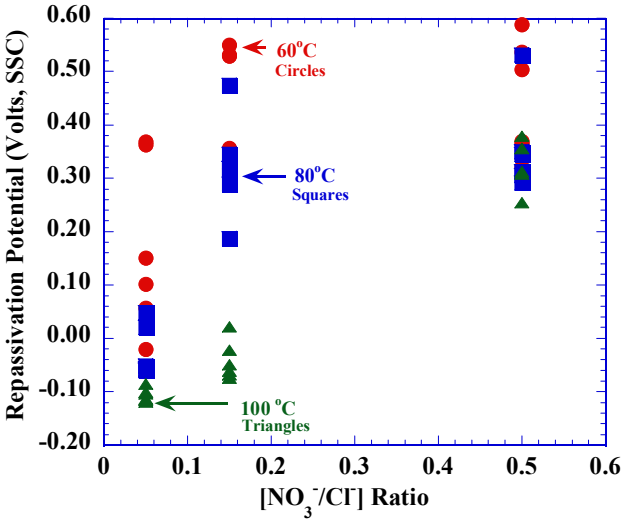

Figure 7. The repassivation potential as a function of $[NO_3^-/Cl^-]$ ratio at $[Cl^-]$ of 1.0, 3.5 and 6.0 molal, and temperatures of 60, 80 and 100 °C.

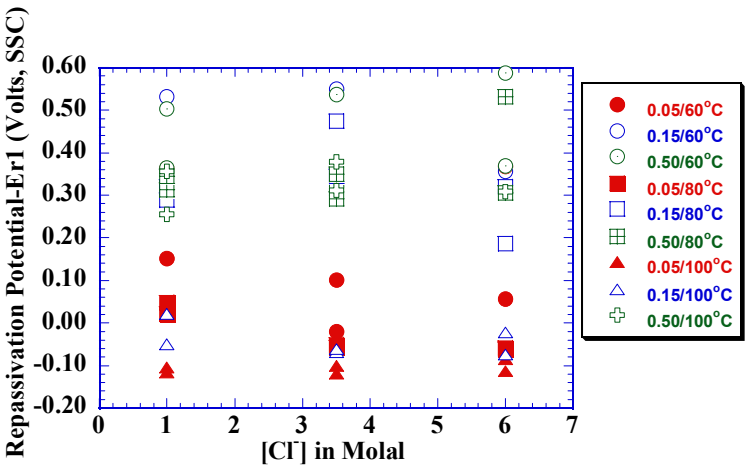

Figure 8. . The repassivation potential as a function of [Cl^-] at [NO_3^-/Cl^-] ratio of 0.05, 0.15 and 0.50, and temperatures of 60, 80 and 100 °C. The legend shows the [NO_3^-/Cl^-] and the temperature for the respective symbols.

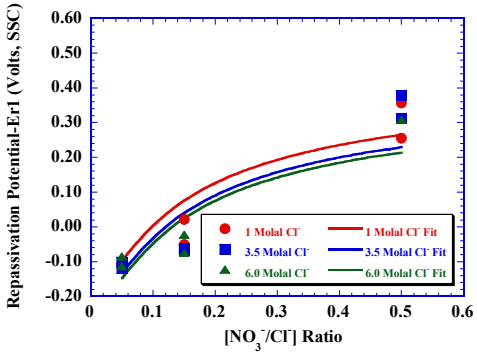

Figure 9. Repassivation potential as a function of [NO_3^-/Cl^-] ratio at 100 °C. The curves describe the repassivation model at T=100°C. Experimental data points at T= 100°C are included (for [Cl^-] = 1.0, 3.5 and 6.0 molal; [NO_3^-/Cl^-] = ratio of 0.05, 0.15 and 0.5).

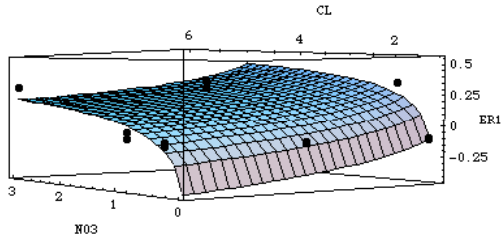

Figure 10. 3-D plot of repassivation potential as a function of [Cl^-] and [NO_3^-] at 100 °C. The surface describes the repassivation model at T=100°C. Experimental data points at T= 100°C are included (for [Cl^-] = 1.0, 3.5 and 6.0 molal; [NO_3^-/Cl^-] = ratio of 0.05, 0.15 and 0.5).

Keywords: Alloy 22, welds, gas tungsten arc weld (GTAW), localized corrosion, inhibition, corrosion potential, repassivation potential, cyclic polarization, nitrate, chloride, temperature.